G protein-gated I_{KACh} channels as therapeutic targets for treatment of sick sinus syndrome and heart block

Pietro Mesirca[a,b,c,1], Isabelle Bidaud[a,b,c], François Briec[d], Stéphane Evain[d], Angelo G. Torrente[a,b,c], Khai Le Quang[d,e], Anne-Laure Leoni[b], Matthias Baudot[a,b,c], Laurine Marger[a,b,c], Antony Chung You Chong[a,b,c], Joël Nargeot[a,b,c], Joerg Striessnig[f], Kevin Wickman[g], Flavien Charpentier[d,e,h,i,2], and Matteo E. Mangoni[a,b,c,1,2]

[a]Département de Physiologie, Institut de Genomique Fonctionnelle, Laboratory of Excellence in Ion Channel Science and Therapeutics, UMR-5203, CNRS, F-34094 Montpellier, France; [b]INSERM U661, F-34094 Montpellier, France; [c]Université de Montpellier, F-34094 Montpellier, France; [d]INSERM, UMR_S1087, l'Institut du Thorax, F-44007 Nantes, France; [e]Université de Nantes, F-44007 Nantes, France; [f]Institute of Pharmacy, Pharmacology and Toxicology and Center of Molecular Biosciences Innsbruck, A-6020 Innsbruck, Austria; [g]Department of Pharmacology, University of Minnesota, Minneapolis, MN 554557; [h]CNRS UMR 6291, l'Institut du Thorax, F-44007 Nantes, France; and [i]Centre Hospitalier Universitaire Nantes, F-44007 Nantes, France

Dysfunction of pacemaker activity in the sinoatrial node (SAN) underlies "sick sinus" syndrome (SSS), a common clinical condition characterized by abnormally low heart rate (bradycardia). If untreated, SSS carries potentially life-threatening symptoms, such as syncope and end-stage organ hypoperfusion. The only currently available therapy for SSS consists of electronic pacemaker implantation. Mice lacking L-type $Ca_v1.3$ Ca^{2+} channels ($Ca_v1.3^{-/-}$) recapitulate several symptoms of SSS in humans, including bradycardia and atrioventricular (AV) dysfunction (heart block). Here, we tested whether genetic ablation or pharmacological inhibition of the muscarinic-gated K^+ channel (I_{KACh}) could rescue SSS and heart block in $Ca_v1.3^{-/-}$ mice. We found that genetic inactivation of I_{KACh} abolished SSS symptoms in $Ca_v1.3^{-/-}$ mice without reducing the relative degree of heart rate regulation. Rescuing of SAN and AV dysfunction could be obtained also by pharmacological inhibition of I_{KACh} either in $Ca_v1.3^{-/-}$ mice or following selective inhibition of $Ca_v1.3$-mediated L-type Ca^{2+} ($I_{Ca,L}$) current in vivo. Ablation of I_{KACh} prevented dysfunction of SAN pacemaker activity by allowing net inward current to flow during the diastolic depolarization phase under cholinergic activation. Our data suggest that patients affected by SSS and heart block may benefit from I_{KACh} suppression achieved by gene therapy or selective pharmacological inhibition.

heart rate regulation | sick sinus syndrome | heart block | GIRK4 | $Ca_v1.3$

Pacemaker activity of the sinoatrial node (SAN) controls heart rate under physiological conditions. Abnormal generation of SAN automaticity underlies "sick sinus" syndrome (SSS), a pathological condition manifested when heart rate is not sufficient to meet the physiological requirements of the organism (1). Typical hallmarks of SSS include SAN bradycardia, chronotropic incompetence, SAN arrest, and/or exit block (1–3). SSS carries incapacitating symptoms, such as fatigue and syncope (1–3). A significant percentage of patients with SSS present also with tachycardia-bradycardia syndrome (3). SSS can also be associated with atrioventricular (AV) conduction block (heart block) (1–3). Although aging is a known intrinsic cause of SSS (4), this disease appears also in the absence of any associated cardiac pathology and displays a genetic legacy (1, 2). Heart disease or drug intake can induce acquired SSS (2). Symptomatic SSS requires the implantation of an electronic pacemaker. SSS accounts for about half of all pacemaker implantations in the United States (5, 6). The incidence of SSS has been forecasted to increase during the next 50 y, particularly in the elder population (7). Furthermore, it has been estimated that at least half of SSS patients will need to be electronically paced (7). Although pacemakers are continuously ameliorated, they remain costly and require lifelong follow-up. Moreover, the implantation of an electronic pacemaker remains difficult in pediatric patients (8). Development of alternative and complementary pharmacological or molecular therapies for SSS management could improve quality of life and limit the need for implantation of electronic pacemakers.

Recently, the genetic bases of some inherited forms of SSS have been elucidated (recently reviewed in 1, 9) with the discovery of mutations in genes encoding for ion channels involved in cardiac automaticity (4, 9, 10). Notably, loss of function of L-type $Ca_v1.3$ Ca^{2+} channels is central in some inherited forms of SSS. For instance, loss of function in $Ca_v1.3$-mediated L-type Ca^{2+} ($I_{Ca,L}$) current causes the sinoatrial node dysfunction and deafness syndrome (SANDD) (10). Affected individuals with SANDD present with profound deafness, bradycardia, and dysfunction of AV conduction (10). Mutation in ankyrin-B causes SSS by reduced membrane targeting of $Ca_v1.3$ channels (11). The relevance of $Ca_v1.3$ channels to SSS is demonstrated also by work on the pathophysiology of congenital heart block, where down-regulation of $Ca_v1.3$ channels by maternal Abs causes heart block in infants (12). Additionally, recent data show that chronic iron overload induces acquired SSS via a reduction in $Ca_v1.3$-mediated $I_{Ca,L}$ (13).

In mice and humans, $Ca_v1.3$ channels are expressed in the SAN, atria, and the AV node but are absent in adult ventricular tissue (14, 15). $Ca_v1.3$-mediated $I_{Ca,L}$ plays a major role in the generation of the diastolic depolarization in SAN and AV

Significance

The "sick sinus" syndrome (SSS) is characterized by abnormal formation and/or propagation of the cardiac impulse. SSS is responsible for about half of the total implantations of electronic pacemakers, which constitute the only currently available therapy for this disorder. We show that genetic ablation or pharmacological inhibition of the muscarinic-gated K^+ channel (I_{KACh}) prevents SSS and abolishes atrioventricular block in model mice without affecting the relative degree of heart rate regulation. We propose that "compensatory" genetic or pharmacological targeting of I_{KACh} channels may constitute a new paradigm for restoring defects in the balance between inward and outward currents in pacemaker cells. Our study may thus open a new therapeutic perspective to manage dysfunction of formation and conduction of the cardiac impulse.

myocytes, thereby constituting important determinants of heart rate and AV conduction velocity (14, 16). The heart rate of mice lacking $Ca_v1.3$ channels ($Ca_v1.3^{-/-}$ mice) fairly recapitulates the hallmarks of SSS and associated symptoms, including bradycardia and tachycardia-bradycardia syndrome (17, 18). In addition, severe AV dysfunction is recorded in $Ca_v1.3^{-/-}$ mice to variable degrees. Typically, these mice show first- and second-degree AV block (16, 17, 19). Complete AV block with dissociated atrial and ventricular rhythms can also be observed in these animals. The phenotype of $Ca_v1.3^{-/-}$ mice thus constitutes a unique model for developing new therapeutic strategies against SSS (10).

The muscarinic-gated K$^+$ channel (I_{KACh}) is involved in the negative chronotropic effect of the parasympathetic nervous system on heart rate (20, 21). Two subunits of the G-protein activated inwardly rectifying K$^+$ channels (GIRK1 and GIRK4) of the GIRK/Kir3 subfamily assemble as heterotetramers to form cardiac I_{KACh} channels (22). Indeed, both $Girk1^{-/-}$ and $Girk4^{-/-}$ mice lack cardiac I_{KACh} (20, 21, 23). We recently showed that silencing of the hyperpolarization-activated current "funny" (I_f) channel in mice induces a complex arrhythmic profile that can be rescued by concurrent genetic ablation of $Girk4$ (24). In this study, we tested the effects of genetic and pharmacological inhibition of I_{KACh} on the $Ca_v1.3^{-/-}$ mouse model of SSS. We found that $Girk4$ ablation or pharmacological inhibition of I_{KACh} rescues SSS and AV dysfunction in $Ca_v1.3^{-/-}$. Thus, our study shows that I_{KACh} targeting may be pursued as a therapeutic strategy for treatment of SSS and heart block.

Results

Pharmacological Inhibition of the Autonomic Nervous System Improved Heart Rate of $Ca_v1.3^{-/-}$ Mice. We first studied heart rate and rhythm by telemetric recording of ECGs in freely moving WT and $Ca_v1.3^{-/-}$ mice (Fig. 1 A and B). WT animals displayed a normal heart rate with no signs of SAN dysfunction or AV block (Fig. 1A). In contrast, $Ca_v1.3^{-/-}$ mice showed typical hallmarks of SSS, including SAN bradycardia, SAN pauses, prolonged AV conduction time (PR interval), and frequent episodes of AV block (Fig. 1B and SI Appendix, Table S1). Pharmacological inhibition of autonomic nervous system input by combined systemic administration of atropine and propranolol significantly reduced heart rate in WT, but not $Ca_v1.3^{-/-}$, mice. Instead, injection of atropine and propranolol abolished SAN pauses and AV blocks in $Ca_v1.3^{-/-}$ mice, suggesting that the activity of the autonomic nervous system induced symptoms of SAN failure and AV dysfunction in these mice (Fig. 1B and SI Appendix, Table S1).

Genetic or Pharmacological Ablation of I_{KACh} Improved SAN Function and AV Conduction in $Ca_v1.3^{-/-}$ Mice. Because inhibition of autonomic input improved SAN and AV conduction of $Ca_v1.3^{-/-}$ mice, we investigated the functional bases of this SSS-rescuing effect. I_{KACh} is a major cardiac effector of the parasympathetic nervous system (20, 21). We thus hypothesized that genetic inactivation of $Girk4$, which leads to a complete loss of cardiac I_{KACh} (20), might reduce the influence of the parasympathetic nervous system on rhythmogenic centers of $Ca_v1.3^{-/-}$ mice, thereby ameliorating the cardiac phenotypes in this mutant mouse strain. Accordingly, we crossed $Ca_v1.3^{-/-}$ mice with $Girk4^{-/-}$ mice and studied heart rate and rhythm in $Girk4^{-/-}$ mice and $Ca_v1.3^{-/-}/Girk4^{-/-}$ double-mutant mice.

As was shown previously (21, 23), the heart rate of $Girk4^{-/-}$ mice was significantly higher than the heart rate of WT controls, and these mice presented normal AV conduction and response to injection of atropine and propranolol (Fig. 1D). The ratio between maximal and minimal heart rates was similar in WT, $Ca_v1.3^{-/-}$, $Ca_v1.3^{-/-}/Girk4^{-/-}$, and $Girk4^{-/-}$ mice, indicating that combined deletion of $Ca_v1.3$ and I_{KACh} did not diminish the relative degree of heart rate regulation (SI Appendix, Fig. S1). Remarkably, both the ventricular rate (RR interval) and SAN rate (PP interval) of $Ca_v1.3^{-/-}/Girk4^{-/-}$ mice were higher than
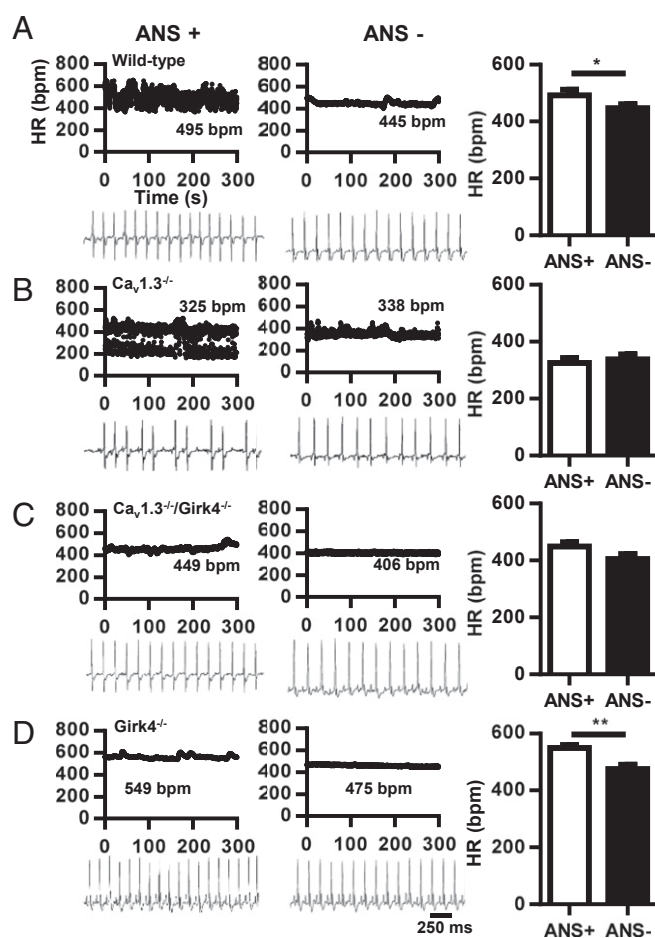

Fig. 1. Dependence of heart block in $Ca_v1.3^{-/-}$ mice on autonomic nervous system (ANS) activity. (A) Dot plot of beat-to-beat variability [heart rate (HR) in bpm] of heart rate (Top) and representative samples of telemetric ECG recordings (Bottom) from WT mice before (Left, ANS+) and after (Right, ANS−) combined injection of atropine (A, 0.5 mg/kg) and propranolol (P, 5 mg/kg). (Right) Histogram shows averaged heart rate before (open bar) and after (filled bar) injection of A + P (n = 13). (B) Same as in A, but for $Ca_v1.3^{-/-}$ mice (n = 8). (C) Same as in A, but for $Ca_v1.3^{-/-}/Girk4^{-/-}$ mice (n = 15). (D) Same as in A, but for $Girk4^{-/-}$ mice (n = 9). Statistics: paired Student's t test. *P < 0.05; **P < 0.01.

the ventricular rate and SAN rate of $Ca_v1.3^{-/-}$ mice and did not differ from the ventricular rate and SAN rate of WT controls (Fig. 1C and SI Appendix, Table S1). $Ca_v1.3^{-/-}/Girk4^{-/-}$ mice also had shorter AV (PR) intervals than their $Ca_v1.3^{-/-}$ counterparts (SI Appendix, Table S1), suggesting that I_{KACh} also exerted a tonic inhibition on impulse conduction of $Ca_v1.3^{-/-}$ animals. Furthermore, the frequency of SAN pauses and AV blocks was reduced by about 10-fold in $Ca_v1.3^{-/-}/Girk4^{-/-}$ mice in comparison to $Ca_v1.3^{-/-}$ mice, showing that $Girk4$ inactivation strongly improved SAN function and AV conduction. Blocking of muscarinic receptors by injection of atropine mimicked the effects of genetic deletion of I_{KACh} in $Ca_v1.3^{-/-}$ mice. Indeed, atropine abolished AV block and drastically reduced the frequency of SAN pauses in $Ca_v1.3^{-/-}$ mice but not in $Ca_v1.3^{-/-}/Girk4^{-/-}$ mice (SI Appendix, Table S2), indicating that the effects of autonomic inhibition of the muscarinic pathway on impulse generation and conduction were entirely dependent on I_{KACh} function. Analysis of heart rate variability (HRV) spectra of $Ca_v1.3^{-/-}$ mice showed high variability in comparison to WT mice, a characteristic attributable to the lower and variable SAN rate and to the presence of intermittent SAN pauses and AV blocks (SI Appendix, Fig. S2). Indeed, concurrent genetic ablation

of I_{KACh} by *Girk4* inactivation significantly reduced the HRV of $Ca_v1.3^{-/-}$ mice (*SI Appendix*, Fig. S2). The HRV of WT and $Ca_v1.3^{-/-}/Girk4^{-/-}$ mice did not significantly differ (*SI Appendix*, Fig. S2 *B and C and Inset*). These observations indicated that genetic ablation of I_{KACh} rescued SSS and heart block of $Ca_v1.3^{-/-}$ mice without reducing heart rate regulation.

The I_{KACh} peptide blocker tertiapin-Q (25) was also effective in rescuing SAN dysfunction and AV block in $Ca_v1.3^{-/-}$ mice (Fig. 2). Tertiapin-Q did not affect the heart rate of WT, $Girk4^{-/-}$, and $Ca_v1.3^{-/-}/Girk4^{-/-}$ mice (Fig. 2 *A–C*). In contrast, injection of tertiapin-Q (5 mg/kg) improved the heart rate of $Ca_v1.3^{-/-}$ mice by increasing SAN rate and abolishing SAN pauses and AV blocks (Fig. 2*D* and *SI Appendix*, Table S3). The AV interval was also shortened by tertiapin-Q.

Injection of tertiapin-Q reduced the HRV of $Ca_v1.3^{-/-}$ mice but did not significantly affect HRV in their $Ca_v1.3^{-/-}/Girk4^{-/-}$ counterparts, indicating that the rescuing effect of this GIRK channel blocker was attributable to I_{KACh} inhibition (*SI Appendix*, Fig. S3). We also tested whether I_{KACh} inhibition could antagonize heart rate slowing and AV block induced by selective pharmacological inhibition of $Ca_v1.3$-mediated $I_{Ca,L}$ (*SI Appendix*,

Fig. S4). To this end, we used mice in which $Ca_v1.2$ channels have been rendered insensitive to dihydropyridines (DHPs) via point mutation, eliminating channel sensitivity to these drugs ($Ca_v1.2^{DHP-/-}$ mice) (26). Indeed, because the mouse heart expresses both $Ca_v1.2$ and $Ca_v1.3$ channels, $Ca_v1.2^{DHP-/-}$ mice permit isolation of the effects of selective inhibition of $Ca_v1.3$-mediated $I_{Ca,L}$ (26, 27). In vivo telemetric recordings of $Ca_v1.2^{DHP-/-}$ mice injected with the DHP blocker amlodipine showed heart rate slowing that was quantitatively similar to the heart rate slowing observed in $Ca_v1.3^{-/-}$ mice (*SI Appendix*, Fig. S4*A*). In addition, amlodipine induced slowing of AV conduction and blocks in $Ca_v1.2^{DHP-/-}$ mice (*SI Appendix*, Fig. S4*B*). In contrast, concurrent injection of tertiapin-Q and amlodipine prevented heart rate slowing and AV blocks, demonstrating that pharmacological inhibition of I_{KACh} was effective in antagonizing drug-induced bradycardia (*SI Appendix*, Fig. S4 *B and C*). Taken together, these observations demonstrated that I_{KACh} activity underlies the phenotypic manifestations of SSS and AV block in $Ca_v1.3^{-/-}$ and $Ca_v1.2^{DHP-/-}$ mice, and that genetic ablation or pharmacological inhibition of this current can rescue heart rhythm.

I_{KACh} Ablation Reduced A_1 Adenosine Receptor-Mediated Bradycardia in $Ca_v1.3^{-/-}$ Mice.

Adenosine slows SAN rate via activation of A_1 adenosine receptors (A_1R) and opening of I_{KACh} channels (20, 28, 29). Release of adenosine can worsen SSS by leading to excessive bradycardia (30). We thus assessed the capability of I_{KACh} ablation to moderate bradycardia induced by A_1R activation in SSS $Ca_v1.3^{-/-}$ mice. We used i.p. injection of the A_1R-selective agonist 2-chloro, N6-cyclopentyl adenosine (CCPA) in $Ca_v1.3^{-/-}$ mice to study SAN dysfunction and AV conduction during A_1R-induced bradycardia (*SI Appendix*, Fig. S5). CCPA (0.1 mg/kg) strongly slowed heart rate in WT and $Ca_v1.3^{-/-}$ mice to a similar degree (55–60%). In addition, CCPA induced deep SAN bradycardia and very low heart rate in $Ca_v1.3^{-/-}$ mice [≈170 beats per minute (bpm)]. However, CCPA was less effective in slowing heart rate in $Ca_v1.3^{-/-}/Girk4^{-/-}$ mice (≈30%), and no deep bradycardia was recorded in these mice. This observation demonstrated the effectiveness of I_{KACh} ablation for preventing excessive A_1R-induced bradycardia in SSS $Ca_v1.3^{-/-}$ mice.

I_{KACh} Ablation Precluded Inducibility of Atrial Tachyarrhythmias in $Ca_v1.3^{-/-}$ Mice.

SSS is often associated with tachycardia-bradycardia syndrome (1, 2). Consistent with previous work on a different strain of $Ca_v1.3^{-/-}$ mice (18), we could induce atrial fibrillation and tachycardia without previous addition of carbachol (31, 32), underscoring the strong susceptibility of SSS $Ca_v1.3^{-/-}$ hearts to atrial tachyarrhythmias (Fig. 3). We thus tested whether *Girk4* inactivation could rescue tachycardia-bradycardia syndrome by improving SAN function and reducing the inducibility of atrial tachyarrhythmias in sedated SSS $Ca_v1.3^{-/-}$ mice. We performed intracardiac ECG recordings in sedated $Ca_v1.3^{-/-}$ and $Ca_v1.3^{-/-}/Girk4^{-/-}$ mice and characterized the properties of atrial rhythm in these strains (Fig. 3 *A–C* and *SI Appendix*, Table S4). Consistent with the improvement in AV conduction observed in $Ca_v1.3^{-/-}/Girk4^{-/-}$ mice in comparison to $Ca_v1.3^{-/-}$ counterparts (Figs. 1 and 2), genetic ablation of I_{KACh} shortened the AV refractory period and the Wenckebach cycle length of $Ca_v1.3^{-/-}$ mice (*SI Appendix*, Table S4). Concurrent inactivation of I_{KACh} also shortened the SAN conduction and recovery time and the SAN-atrium conduction time in $Ca_v1.3^{-/-}$ mice, which indicated improvement of the SAN function (*SI Appendix*, Table S5). Intracardiac atrial stimulation induced atrial fibrillation (Fig. 3*A, Top*) or atrial tachycardia (Fig. 3*A, Bottom*) in eight of 12 $Ca_v1.3^{-/-}$ mice tested (Fig. 3*D* and *SI Appendix*, Table S6). All arrhythmias in $Ca_v1.3^{-/-}$ mice terminated spontaneously. In contrast, atrial arrhythmia could be elicited in only two of 10 $Ca_v1.3^{-/-}/Girk4^{-/-}$ mice (Fig. 3*D* and *SI Appendix*, Table S6). Taken together, these observations indicated that I_{KACh} deletion could rescue tachycardia-bradycardia syndrome and AV block in the $Ca_v1.3^{-/-}$ mouse model of SSS.
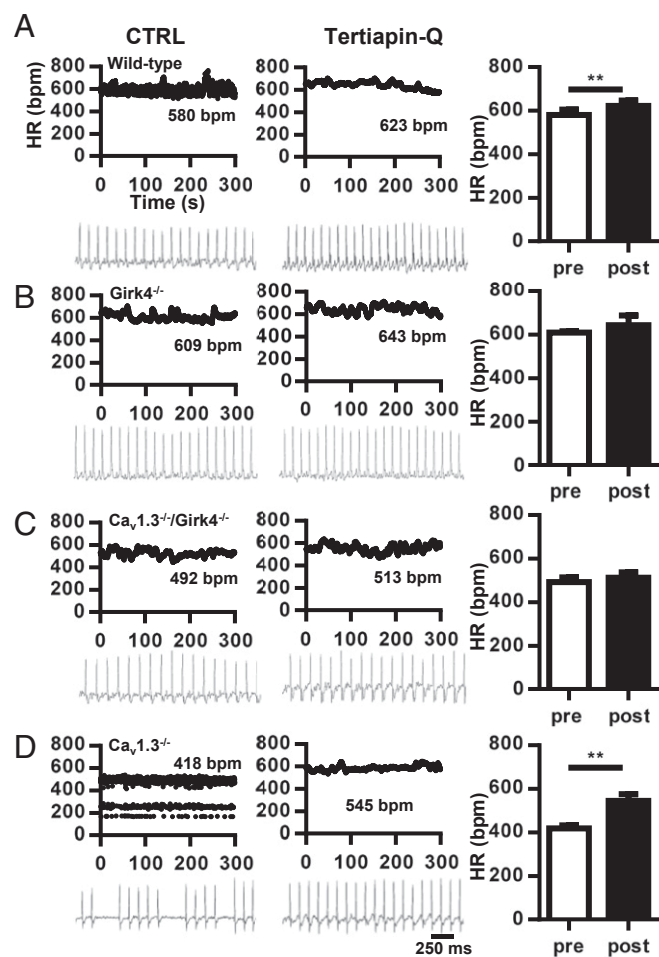

Fig. 2. Effect of the I_{KACh} blocker tertiapin-Q on bradycardia and heart block in $Ca_v1.3^{-/-}$ mice. (*A*) Dot plot of beat-to-beat variability (HR in bpm) of heart rate (*Top*) and representative samples of telemetric ECG recordings (*Bottom*) from WT mice before (*Left*) and after (*Center*) i.p. injection of tertiapin-Q (5 mg/kg) in WT mice. (*Right*) Histogram shows averaged heart rates before (open bar) and after (filled bar) injection of tertiapin-Q (n = 4). (*B*) Same as in *A*, but for $Girk4^{-/-}$ mice (n = 4). (*C*) Same as in *A*, but for $Ca_v1.3^{-/-}/Girk4^{-/-}$ mice (n = 4). (*D*) Same as in *A*, but for $Ca_v1.3^{-/-}$ mice (n = 5). Statistics: paired Student's *t* test. **$P < 0.01$.
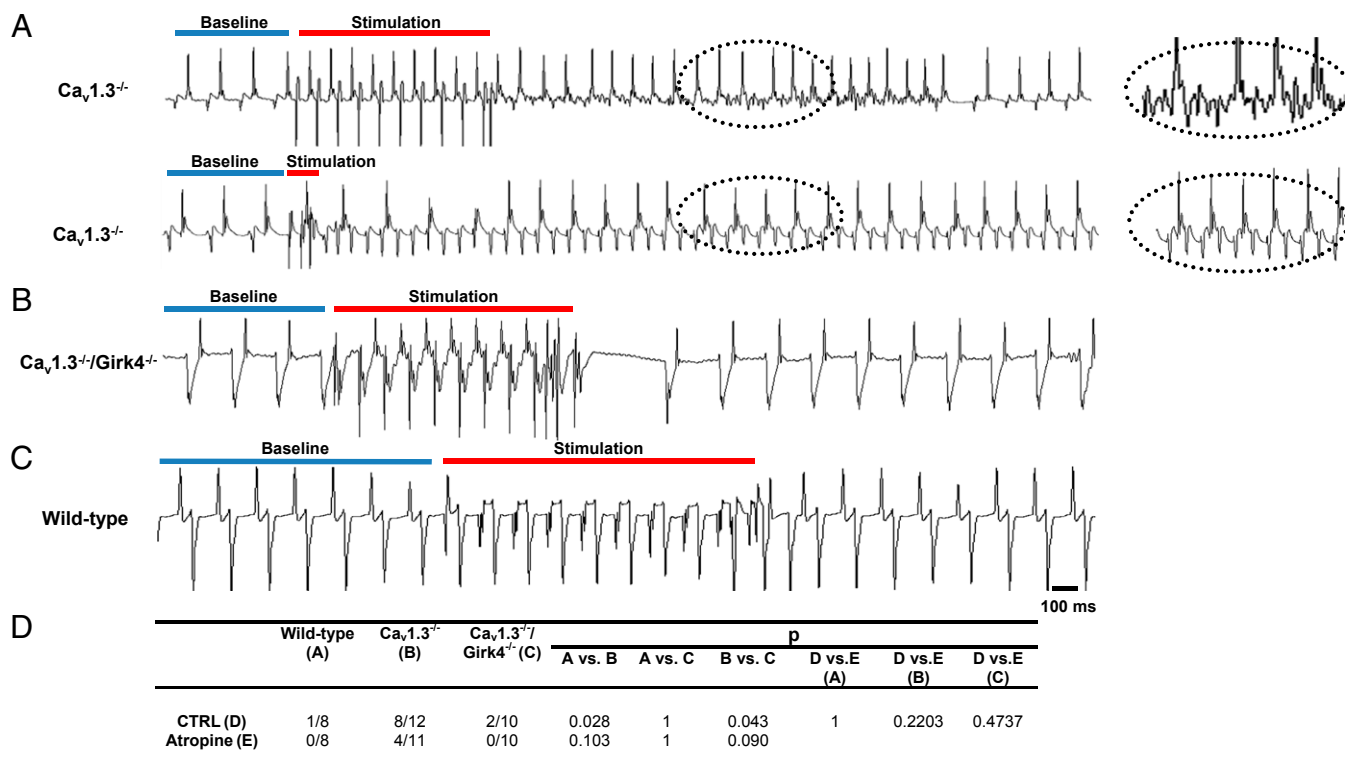
Fig. 3. I_{KACh} ablation suppresses atrial tachyarrhythmias in $Ca_v1.3^{-/-}$ mice. (A) Representative examples of pacing-induced atrial fibrillation (*Top*) and atrial tachycardia (*Bottom*) in $Ca_v1.3^{-/-}$ mice. Traces represent intracardiac electrogram recordings before pacing (baseline, blue bar), during pacing (stimulation, red bar), and after pacing. (*Insets*) Close-up views of arrhythmias recorded after pacing. No atrial fibrillation or atrial tachycardia was recorded in $Ca_v1.3^{-/-}/Girk4^{-/-}$ (B) and WT (C) mice after intracardiac atrial stimulation. (D) Statistical analysis of the incidence of pacing-induced arrhythmias. Statistics: Fisher's exact test. CTRL, control.

I_{KACh} Ablation Normalized Action Potential Duration in $Ca_v1.3^{-/-}$ Atrial Myocytes. Supraventricular arrhythmia in $Ca_v1.3^{-/-}$ mice could be due to an alteration in the atrial action potential. We thus compared the action potential duration of atrial myocytes in the different genotypes to test the ability of I_{KACh} ablation to normalize this parameter of atrial excitability (Fig. 4). WT and $Girk4^{-/-}$ myocytes displayed similar action potential durations (Fig. 4A). In contrast, $Ca_v1.3^{-/-}$ myocytes had shortened action potential durations. However, $Ca_v1.3^{-/-}/Girk4^{-/-}$ myocytes displayed normal action potential duration, suggesting that I_{KACh} contributes to action potential repolarization even in the absence of ACh (Fig. 4 A–C). Consistent with this hypothesis, tertiapin-Q significantly prolonged the action potential duration of WT and $Ca_v1.3^{-/-}$ myocytes but had no effect on $Girk4^{-/-}$ and $Ca_v1.3^{-/-}/Girk4^{-/-}$ myocytes (*SI Appendix*, Fig. S6). Comparison between I_{KACh} densities of WT and $Ca_v1.3^{-/-}$ myocytes showed that SAN myocytes from KO mice had reduced I_{KACh} (Fig. 4 D–H), negating the difference in I_{KACh} density between SAN and atrial myocytes observed in WT mice. These observations showed that genetic ablation or pharmacological blockade of I_{KACh} restored the normal action potential waveform of atrial $Ca_v1.3^{-/-}$ myocytes.

I_{KACh} Ablation Rescued SSS of $Ca_v1.3^{-/-}$ Hearts by Reducing ACh-Induced SAN Bradycardia and AV Block. Because suppression of I_{KACh} significantly reduces the muscarinic regulation of pacemaker activity in SAN myocytes (21), we hypothesized that improvement of SAN rate and AV conduction in $Ca_v1.3^{-/-}/Girk4^{-/-}$ mice was due to a decrease in the sensitivity of SAN automaticity and AV conduction to ACh. We thus tested the chronotropic and dromotropic effects of ACh on heart rate and AV conduction in isolated Langendorff-perfused hearts (Fig. 5). Perfusion with 0.3 µM ACh similarly reduced the

beating rate of WT and $Ca_v1.3^{-/-}$ hearts (34% in WT, 39% in $Ca_v1.3^{-/-}$). In contrast, $Ca_v1.3^{-/-}/Girk4^{-/-}$ hearts showed a reduced chronotropic response to ACh, which was similar to the chronotropic response of $Girk4^{-/-}$ hearts (16% in $Girk4^{-/-}$, 13% in $Ca_v1.3^{-/-}/Girk4^{-/-}$; Fig. 5). These results indicated that I_{KACh} ablation was the dominant factor in determining the sensitivity of isolated hearts to ACh. ACh had a similar effect (35–37%) on AV conduction time (PR interval) of WT and $Girk4^{-/-}$ hearts. In contrast, the PR interval of $Ca_v1.3^{-/-}$ hearts was more than doubled by ACh perfusion (77%), whereas the negative dromotropic effect of ACh on $Ca_v1.3^{-/-}/Girk4^{-/-}$ hearts was similar to the dromotropic effect observed in $Girk4^{-/-}$ hearts (29%). These observations indicated that I_{KACh} ablation reduced ACh-mediated negative chronotropic and dromotropic effects, preventing excessive rate reduction and AV block in SSS $Ca_v1.3^{-/-}$ hearts.

SAN Myocytes from $Ca_v1.3^{-/-}/Girk4^{-/-}$ Mice Have Reduced Muscarinic Regulation of Pacemaker Activity. The prominent reduction of ACh-induced SAN dysfunction in isolated SSS $Ca_v1.3^{-/-}$ hearts prompted us to investigate the impact of I_{KACh} ablation on isolated pacemaker myocytes (Fig. 6). Perfusion of spontaneously beating myocytes with ACh dose-dependently decreased the beating rate of WT, $Ca_v1.3^{-/-}$, and $Girk4^{-/-}$ myocytes (Fig. 6 A, B, and D and *SI Appendix*, Table S7). In contrast, $Ca_v1.3^{-/-}/Girk4^{-/-}$ SAN myocytes did not show a significant ACh-mediated rate reduction, even in response to 0.05 µM ACh, a concentration sufficient to stop pacemaking in all WT and $Ca_v1.3^{-/-}$ myocytes (Fig. 6C). This observation indicated that I_{KACh} ablation reduced the negative chronotropic effect mediated by ACh on pacemaker activity in $Ca_v1.3^{-/-}$ myocytes. I_{KACh} ablation also increased the basal spontaneous pacing rate of $Ca_v1.3^{-/-}/Girk4^{-/-}$
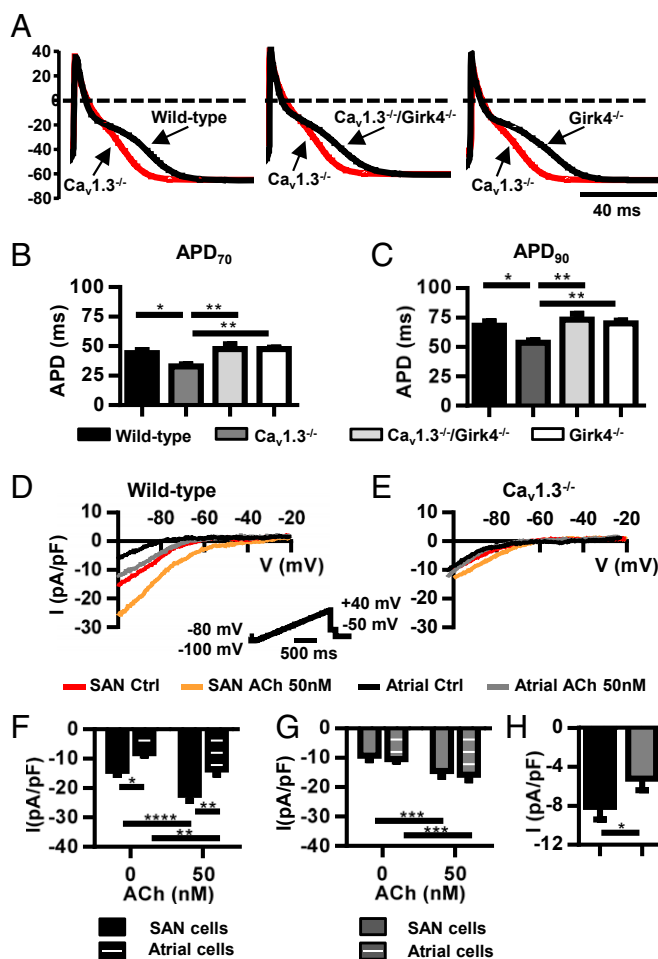
Fig. 4. Normalization of action potential duration of $Ca_v1.3^{-/-}$ atrial myocytes after I_{KACh} ablation. (A) Action potential sample traces of $Ca_v1.3^{-/-}$ atrial myocytes (red trace) overlapped with action potentials from WT (*Left*), $Ca_v1.3^{-/-}/Girk4^{-/-}$ (*Middle*), or $Girk4^{-/-}$ myocytes (*Right*). Action potential durations at 70% (*B*, APD_{70}) and 90% (*C*, APD_{90}) of repolarization in $n = 14$ WT, $n = 13$ $Ca_v1.3^{-/-}$, $n = 19$ $Ca_v1.3^{-/-}/Girk4^{-/-}$, and $n = 17$ $Girk4^{-/-}$ myocytes are shown. Statistics: one-way ANOVA followed by Holm–Sidak's multiple comparisons test. Sample traces of I_{KACh} before and after ACh perfusion (0.05 μM) in SAN and atrial myocytes of WT mice (*D*) and $Ca_v1.3^{-/-}$ mice (*E*) are shown. (*D, Inset*) Voltage clamp protocol. Averaged I_{KACh} densities before and after ACh are shown in the bar plots for SAN ($n = 14$) and atrial WT myocytes ($n = 11$) (*F*) and SAN ($n = 18$) and atrial $Ca_v1.3^{-/-}$ myocytes ($n = 15$) (*G*). (*H*) I_{KACh} induced by ACh perfusion measured by subtracting the basal current from the basal current in ACh. Statistics: two-way ANOVA followed by Sidak's multiple comparisons test. *$P < 0.05$; **$P < 0.01$; ***$P < 0.001$; ****$P < 0.0001$.

myocytes in comparison to the basal spontaneous pacing rate of their $Ca_v1.3^{-/-}$ counterparts (*SI Appendix*, Table S7), suggesting that some I_{KACh} channels are open in the SAN in the absence of exogenous ACh.

ACh decreased the pacemaker activity of WT SAN myocytes by reducing the slope of the diastolic depolarization and by increasing the frequency of delayed after-depolarizations (DADs; Fig. 6*A* and *SI Appendix*, Fig. S7), low-amplitude depolarizations of the membrane potential (≥ 10 mV) that failed to reach the action potential threshold. In contrast, ACh decreased pacemaker activity of $Ca_v1.3^{-/-}$ myocytes by increasing the incidence of DADs, leaving unaffected the slope of the diastolic depolarization (Fig. 6*B* and *SI Appendix*, Table S7), suggesting that formation of DADs, rather than normal action potentials, constituted the mechanism underlying ACh-induced SAN dysfunc-

tion in SSS $Ca_v1.3^{-/-}$ hearts. In agreement with this hypothesis, an increase in the frequency of DADs could be observed in $Ca_v1.3^{-/-}/Girk4^{-/-}$ myocytes at high concentrations of ACh (0.05 μM; *SI Appendix*, Fig. S7), accounting for the rescuing of the ACh-induced negative chronotropic effect recorded in $Ca_v1.3^{-/-}$ myocytes. Taken together, these data demonstrated that the rescuing of SSS observed in $Ca_v1.3^{-/-}/Girk4^{-/-}$ mice was due to a strong reduction in the sensitivity of SAN pacemaker activity to ACh-mediated negative chronotropy and that $Ca_v1.3$-mediated $I_{Ca,L}$ contributed to the cholinergic regulation of pacemaker activity in WT and $Girk4^{-/-}$ SAN.

Genetic or Pharmacological Ablation of I_{KACh} Prevented the Formation of $[Ca^{2+}]_i$ Waves in $Ca_v1.3^{-/-}$ SAN Myocytes. The high incidence of DADs recorded during pacemaker activity under perfusion of ACh suggested altered intracellular Ca^{2+} ($[Ca^{2+}]_i$) dynamics and the frequency of $[Ca^{2+}]_i$ waves in $Ca_v1.3^{-/-}$ myocytes. We thus used confocal line scan imaging of Fluo-4–loaded cells to test whether ablation of I_{KACh} could rescue $[Ca^{2+}]_i$ dynamics in SAN myocytes from $Ca_v1.3^{-/-}$ mice (Fig. 7). Consistent with the slow pacemaker activity observed under current-clamp conditions (Fig. 6), we recorded slower frequency of spontaneous $[Ca^{2+}]_i$ transients in $Ca_v1.3^{-/-}$ SAN myocytes in comparison to the spontaneous $[Ca^{2+}]_i$ transients of WT, $Girk4^{-/-}$, and $Ca_v1.3^{-/-}/Girk4^{-/-}$ myocytes (Fig. 7 *A–D*, *Left* and *Middle*).

In WT, $Ca_v1.3^{-/-}$, and $Girk4^{-/-}$ myocytes, ACh reduced the frequency of spontaneous $[Ca^{2+}]_i$ transients and induced the formation of $[Ca^{2+}]_i$ waves (Fig. 7 *A*, *B*, and *D*). In $Ca_v1.3^{-/-}/Girk4^{-/-}$ SAN myocytes, the rate of spontaneous $[Ca^{2+}]_i$ transients was similar to the rate of spontaneous $[Ca^{2+}]_i$ transients of WT and $Girk4^{-/-}$ cells, and the frequency of $[Ca^{2+}]_i$ waves was lower than the frequency of $[Ca^{2+}]_i$ waves recorded in the other genotypes (Fig. 7*C*). In $Ca_v1.3^{-/-}/Girk4^{-/-}$ myocytes, ACh failed to decrease the frequency of spontaneous $[Ca^{2+}]_i$ transients and to increase the frequency of $[Ca^{2+}]_i$ waves (Fig. 7*C*). Consistent with this observation, ACh did not decrease the frequency of spontaneous $[Ca^{2+}]_i$ transients or increase $[Ca^{2+}]_i$ waves in $Ca_v1.3^{-/-}$ cells when tertiapin-Q was added to the perfusion medium (*SI Appendix*, Fig. S8).

Because I_{KACh} ablation in $Ca_v1.3^{-/-}/Girk4^{-/-}$ mice allowed the formation of cell-wide $[Ca^{2+}]_i$ transients instead of $[Ca^{2+}]_i$ waves, we tested whether this rescuing effect required functional ryanodine receptor (RyR)-dependent $[Ca^{2+}]_i$ release. The dose–response relationship of the frequency of spontaneous $[Ca^{2+}]_i$ transients to ryanodine showed a differential effect between WT and $Girk4^{-/-}$ SAN myocytes (*SI Appendix*, Fig. S9). Indeed, whereas 1 μM ryanodine drastically reduced the frequency of spontaneous $[Ca^{2+}]_i$ transients in WT SAN myocytes, it remained higher in $Girk4^{-/-}$ myocytes (*SI Appendix*, Fig. S9*A*). A saturating concentration of ryanodine (3 μM) that completely disabled RyR-dependent Ca^{2+} release drastically reduced spontaneous $[Ca^{2+}]_i$ transients and action potentials in both WT and $Girk4^{-/-}$ SAN myocytes, indicating that pacemaker activity required RyR-dependent Ca^{2+} release (*SI Appendix*, Fig. S9*B*).

Concurrent perfusion of a moderate concentration of ryanodine (0.3 μM) with ACh (0.01 μM) did not significantly affect the frequency of spontaneous $[Ca^{2+}]_i$ transients in $Girk4^{-/-}$ myocytes. This observation suggested that ablation of I_{KACh} could rescue the loss of RyR-dependent Ca^{2+} release in WT SAN myocytes at moderate concentrations of ryanodine (*SI Appendix*, Figs. S10 and S11). Moreover, the relative insensitivity to 0.01 μM ACh of ryanodine-treated $Girk4^{-/-}$ SAN myocytes suggested that regulation of RyR-dependent Ca^{2+} release contributes to cholinergic regulation of pacemaking. In contrast, the frequencies of spontaneous $[Ca^{2+}]_i$ transients of WT, $Ca_v1.3^{-/-}$, and $Ca_v1.3^{-/-}/Girk4^{-/-}$ SAN myocytes were strongly reduced by ryanodine and ACh, and to comparable levels (*SI Appendix*, Figs. S10 and S11). These observations showed that although I_{KACh}
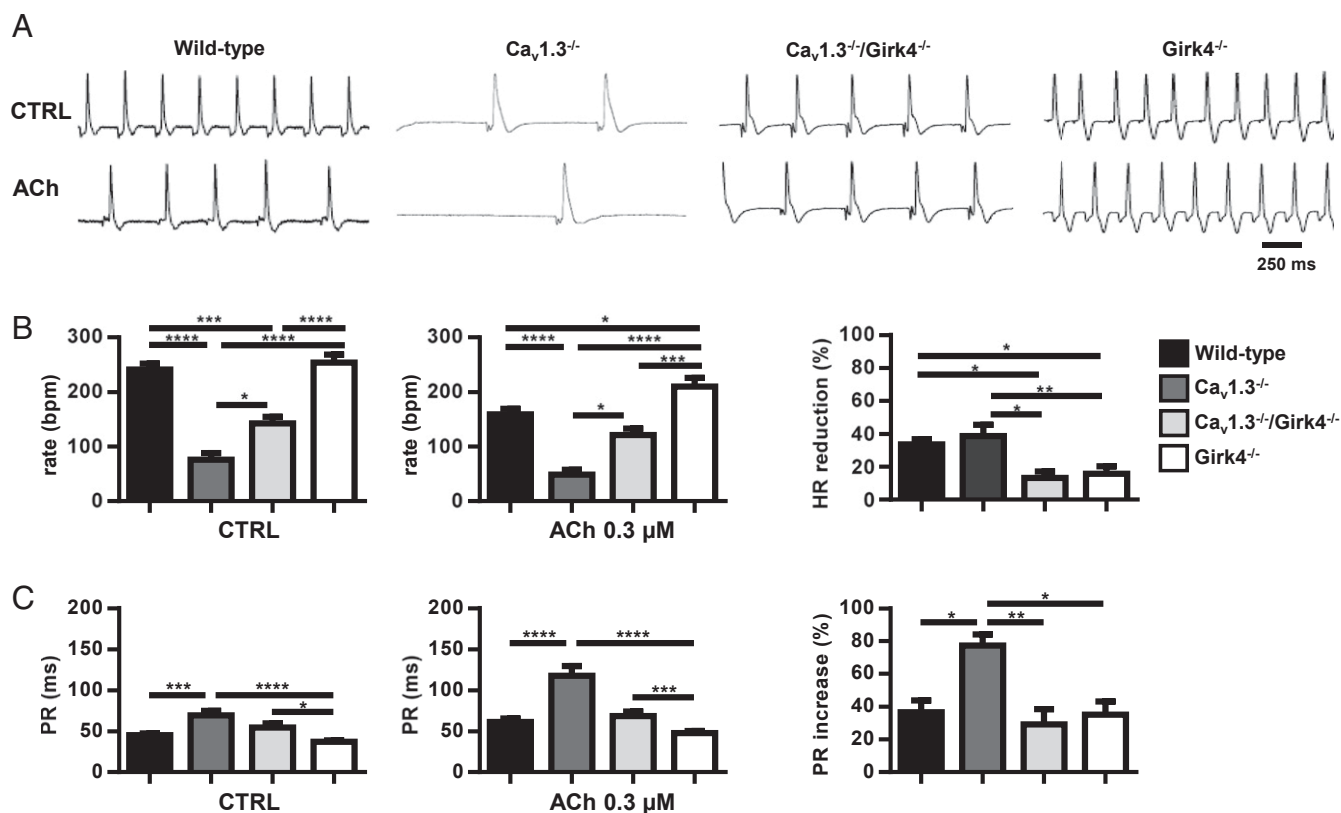
Fig. 5. ACh (0.3 μM) effect on heart rate and AV conduction in isolated Langendorff-perfused hearts. (*A*) Representative traces in CTRL conditions (*Top*) and ACh-perfused (*Bottom*) hearts from WT, $Ca_v1.3^{-/-}$, $Ca_v1.3^{-/-}/Girk4^{-/-}$, and $Girk4^{-/-}$ mice. (*B*) Mean value of heart rate in control (*Left*; $n = 13$ WT, $n = 8$ $Ca_v1.3^{-/-}$, $n = 7$ $Ca_v1.3^{-/-}/Girk4^{-/-}$, and $n = 16$ $Girk4^{-/-}$ hearts) and ACh-perfused (*Middle*; $n = 12$ WT, $n = 9$ $Ca_v1.3^{-/-}$, $n = 7$ $Ca_v1.3^{-/-}/Girk4^{-/-}$, and $n = 16$ $Girk4^{-/-}$ hearts) hearts. (*Right*) ACh-dependent heart rate reduction expressed as percentage measured in the different mouse strains studied. (*C*) Mean value of PR interval in Tyrode's solution ($n = 9$ WT, $n = 9$ $Ca_v1.3^{-/-}$, $n = 8$ $Ca_v1.3^{-/-}/Girk4^{-/-}$, and $n = 10$ $Girk4^{-/-}$ hearts; *Left*) and ACh ($n = 9$ WT, $n = 9$ $Ca_v1.3^{-/-}$, $n = 8$ $Ca_v1.3^{-/-}/Girk4^{-/-}$, and $n = 8$ $Girk4^{-/-}$ hearts; *Middle*) perfused hearts. (*Right*) ACh-dependent PR interval reduction expressed as percentage. Statistics: one-way ANOVA followed by Tukey's multiple comparisons test. *$P < 0.05$; **$P < 0.01$; ***$P < 0.001$; ****$P < 0.0001$.

ablation could antagonize the negative chronotropic effect induced by ryanodine and ACh in WT cells containing functional $Ca_v1.3$-mediated $I_{Ca,L}$, rescuing of automaticity in $Ca_v1.3^{-/-}$ SAN myocytes under ACh required fully functional RyR-dependent Ca^{2+} release.

I_{KACh} Ablation Maintained the Diastolic Current in the Inward Direction During Muscarinic Activation. Pacemaker activity requires the presence of a net inward current to sustain the diastolic depolarization. Because cholinergic activation of I_{KACh} generates an outward current, we hypothesized that upon parasympathetic activation, the lack of $Ca_v1.3$-mediated $I_{Ca,L}$ shifts the net membrane current of SAN and AV node myocytes in the outward direction, thereby inducing SAN failure and AV block. We thus tested the effects of I_{KACh} ablation on the total diastolic current by using a train of spontaneous action potentials recorded in WT SAN cells as voltage-clamp commands (Fig. 8). $Ca_v1.3^{-/-}$ SAN myocytes showed reduced total inward diastolic current in comparison to their WT counterparts under basal conditions (Fig. 8 *A* and *B*). Perfusion with ACh (0.05 μM) shifted the direction of the diastolic current from inward to outward in WT and $Ca_v1.3^{-/-}$ myocytes (Fig. 8 *A* and *B*). ACh reduced the diastolic current also in $Girk4^{-/-}$ myocytes, but the net current direction remained inward (Fig. 8*C*). This evidence is in line with current-clamp experiments that showed arrest of cell pacemaker activity at this ACh concentration in WT and $Ca_v1.3^{-/-}$ myocytes, but not in $Girk4^{-/-}$ cells (Fig. 6). In contrast, ACh did not significantly affect the diastolic current in $Ca_v1.3^{-/-}/Girk4^{-/-}$ SAN myocytes at any concentration tested (Fig. 8*D*). This observation was consistent

with the strong reduction of the cholinergic regulation of cell pacemaker activity of $Ca_v1.3^{-/-}/Girk4^{-/-}$ SAN myocytes (Fig. 6) and indicates that, together with I_{KACh} and RyR-dependent $[Ca^{2+}]_i$ release, $Ca_v1.3$-mediated $I_{Ca,L}$ is an effector of cholinergic regulation of pacemaker activity. These results indicate that genetic ablation or pharmacological inhibition of I_{KACh} prevented ACh-mediated slowing of pacemaker activity by maintaining the net diastolic current in the inward direction and preventing the formation of $[Ca^{2+}]_i$ waves (Fig. 7).

Discussion

In this study, we demonstrated that genetic ablation or pharmacological inhibition of I_{KACh} strongly ameliorates SAN dysfunction, prevents tachycardia-bradycardia syndrome, and normalizes AV impulse conduction in a mouse model of human SSS. I_{KACh} ablation did not reduce the relative degree of heart rate regulation, and we did not observe episodes of ventricular arrhythmia in $Ca_v1.3^{-/-}/Girk4^{-/-}$ or $Ca_v1.3^{-/-}$ mice treated with tertiapin-Q. These observations suggest that I_{KACh} inhibition preserves the capability of the organism to regulate heart rate without being, by itself, proarrhythmic. At present, no pharmacological therapy is available to improve heart rate and AV conduction in the context of SSS. Thus, our work suggests that genetic or pharmacological targeting of I_{KACh} channels may be efficacious in the management of SSS and heart block.

Several studies highlight the importance of $Ca_v1.3$-mediated $I_{Ca,L}$ in human pathologies of heart rhythm and indicate that $Ca_v1.3^{-/-}$ mice constitute a suitable preclinical model for testing
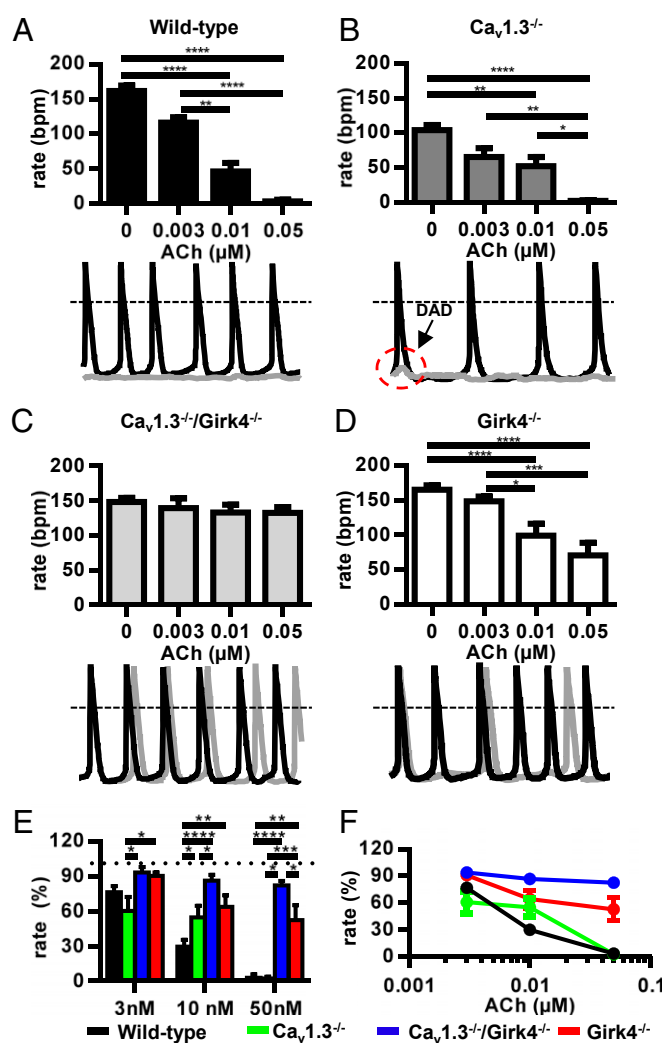
Fig. 6. Slowing of pacemaker activity of $Ca_v1.3^{-/-}$ SAN myocytes after ACh inhibition. Histograms of spontaneous action potential rate recorded in control conditions and after perfusion of ACh at the indicated doses in SAN myocytes from WT (*A, Top*), $Ca_v1.3^{-/-}$ (*B, Top*), $Ca_v1.3^{-/-}/Girk4^{-/-}$ (*C, Top*), and $n = 9$ $Girk4^{-/-}$ (*D, Top*) mice. Examples of spontaneous SAN cells action potentials recorded from WT (*A, Bottom*), $Ca_v1.3^{-/-}$ (*B, Bottom*), $Ca_v1.3^{-/-}/Girk4^{-/-}$ (*C, Bottom*), and $Girk4^{-/-}$ (*D, Bottom*) mice in control conditions (black traces) and after perfusion of ACh (0.05 μM, gray traces). (*A–D*) Statistics: one-way ANOVA followed by Tukey's multiple comparisons test. (*E* and *F*) Dose–response relation of the percentages of rate reduction at different doses ACh in SAN cells isolated from WT, $Ca_v1.3^{-/-}$, $Ca_v1.3^{-/-}/Girk4^{-/-}$, and $Girk4^{-/-}$ mice. (*E*) Statistics: two-way ANOVA followed by Tukey's multiple comparisons test. The number of SAN cells measured is reported in *SI Appendix*, Table S7 for each genotype and ACh concentration. *$P < 0.05$; **$P < 0.01$; ***$P < 0.001$; ****$P < 0.0001$.

new therapeutic strategies for SSS and heart block. Indeed, $Ca_v1.3^{-/-}$ mice present several aspects of human SSS (10, 18), including SAN dysfunction (1, 2) and tachycardia-bradycardia syndrome (33, 34). In addition, $Ca_v1.3^{-/-}$ mice reproduce severe AV dysfunction typical of human congenital heart block (16).

Previous studies demonstrated that $Ca_v1.3$-mediated $I_{Ca,L}$ plays a major role in the determination of heart rate and impulse conduction in mice and humans (10, 11, 14, 16, 17, 19). However, despite the importance of $Ca_v1.3$-mediated $I_{Ca,L}$ in determining the rate of the diastolic depolarization in isolated SAN and AV node myocytes (14, 16), it was unclear how $Ca_v1.3$ loss of function translates into SSS in vivo. In this respect, we show, for the first time to our knowledge, that SSS symptoms and AV block in vivo

in $Ca_v1.3^{-/-}$ mice depend upon I_{KACh} and that targeted inhibition of these channels can rescue SSS. Indeed, we did not record SAN failure or AV block in $Ca_v1.3^{-/-}/Girk4^{-/-}$ mice, and we did not detect SAN failure or AV block following injection of tertiapin-Q in $Ca_v1.3^{-/-}$ or $Ca_v1.2^{DHP-/-}$ mice treated with amlodipine. In this respect, the rescue of bradycardia was particularly striking, because the heart rate of all these "rescued" mice was normalized, reaching values that were close to the values recorded in WT or control uninjected $Ca_v1.2^{DHP-/-}$ mice (*SI Appendix*, Fig. S4). This result indicates that structural or functional remodeling of rhythmogenic centers of $Ca_v1.3^{-/-}$ and $Ca_v1.3^{-/-}/Girk4^{-/-}$ mice is not the primary mechanism mediating the rescuing effect on heart rate by I_{KACh} targeting.

Normal SAN pacemaker activity is generated by a complex interplay between inward ionic currents of the plasma membrane, such as $Ca_v1.3$-mediated $I_{Ca,L}$, $Ca_v3.1$-mediated T-type Ca^{2+} current ($I_{Ca,T}$), hyperpolarization-activated current "funny" (I_f), and Na^+/Ca^{2+} exchanger current (I_{NCX}) activated by RyR-dependent $[Ca^{2+}]_i$ release (35–37). With regard to the SAN pacemaker mechanism, two mutually connected concepts emerge from our findings. First, although I_{KACh} constitutes an important mechanism in heart rate control (20, 21), its activity becomes detrimental for cardiac automaticity and rhythm following loss of function of ion channels, contributing to the generation of the diastolic depolarization (24) (Figs. 1 and 2). Second, our study indicates that an intrinsic functional redundancy among ion channels involved in the SAN pacemaker mechanism allows viable heart rate and heart rate regulation without SSS symptoms, provided that I_{KACh} activity is abolished or suppressed (Figs. 1–3 and 8).

Rescuing of tachycardia-bradycardia syndrome in $Ca_v1.3^{-/-}/Girk4^{-/-}$ demonstrates that I_{KACh} activity constitutes a major mechanism underlying SSS symptoms and associated arrhythmias. In this respect, atrial action potential shortening and reduced $I_{Ca,L}$ are important cellular mechanisms underlying atrial fibrillation (38–40). Similar to what is observed in experimental animal models of paroxystic atrial fibrillation lacking SSS and heart block (41–44), normalization of the atrial action potential duration of $Ca_v1.3^{-/-}$ myocytes can account for prevention of atrial tachyarrhythmia in this model of SSS. However, because $Ca_v1.3^{-/-}$ mice have an intrinsically low SAN rate, we cannot exclude the possibility that SAN dysfunction in $Ca_v1.3^{-/-}$ mice also contributes to the susceptibility to atrial arrhythmias. This mechanism would still be consistent with the observed rescuing of tachycardia-bradycardia syndrome in $Ca_v1.3^{-/-}$ mice, because I_{KACh} ablation also prevented SAN dysfunction (*SI Appendix*, Table S4).

In comparison to individuals with sinus rhythm, agonist-independent constitutive I_{KACh} activity (45) and reduced expression of I_{KACh} (46) in atrial myocytes are typical of patients with chronic atrial fibrillation. $Ca_v1.3^{-/-}$ SAN myocytes showed reduced basal I_{KACh} and diminished density of agonist-induced current in comparison to WT myocytes (Fig. 4). I_{KACh} downregulation in pacemaker tissue and/or atria can thus constitute a common compensatory mechanism between mice and humans to counteract I_{KACh}-induced SSS symptoms or atrial arrhythmias.

We attribute the rescue of SAN function in $Ca_v1.3^{-/-}$ mice to the ability of I_{KACh} ablation or inhibition to prevent ACh-induced formation of $[Ca^{2+}]_i$ waves (Fig. 7) and DADs (Fig. 6), as well as to the shift of the total diastolic membrane current to the inward direction under ACh in $Ca_v1.3^{-/-}/Girk4^{-/-}$ in comparison to $Ca_v1.3^{-/-}$ pacemaker myocytes (Fig. 8 *A–D*). This view can be summarized by a general model in which pacemaker activity is determined by the balance between inward currents contributing to the diastolic depolarization and I_{KACh}, which brakes automaticity by supplying outward current (Fig. 8*E*). Loss of $Ca_v1.3$-mediated $I_{Ca,L}$ generates an imbalance between inward and outward currents that induces dysfunction of pacemaker activity. Normal pacemaking can thus be restored by genetic or pharmacological inhibition of I_{KACh}. Under these conditions, the
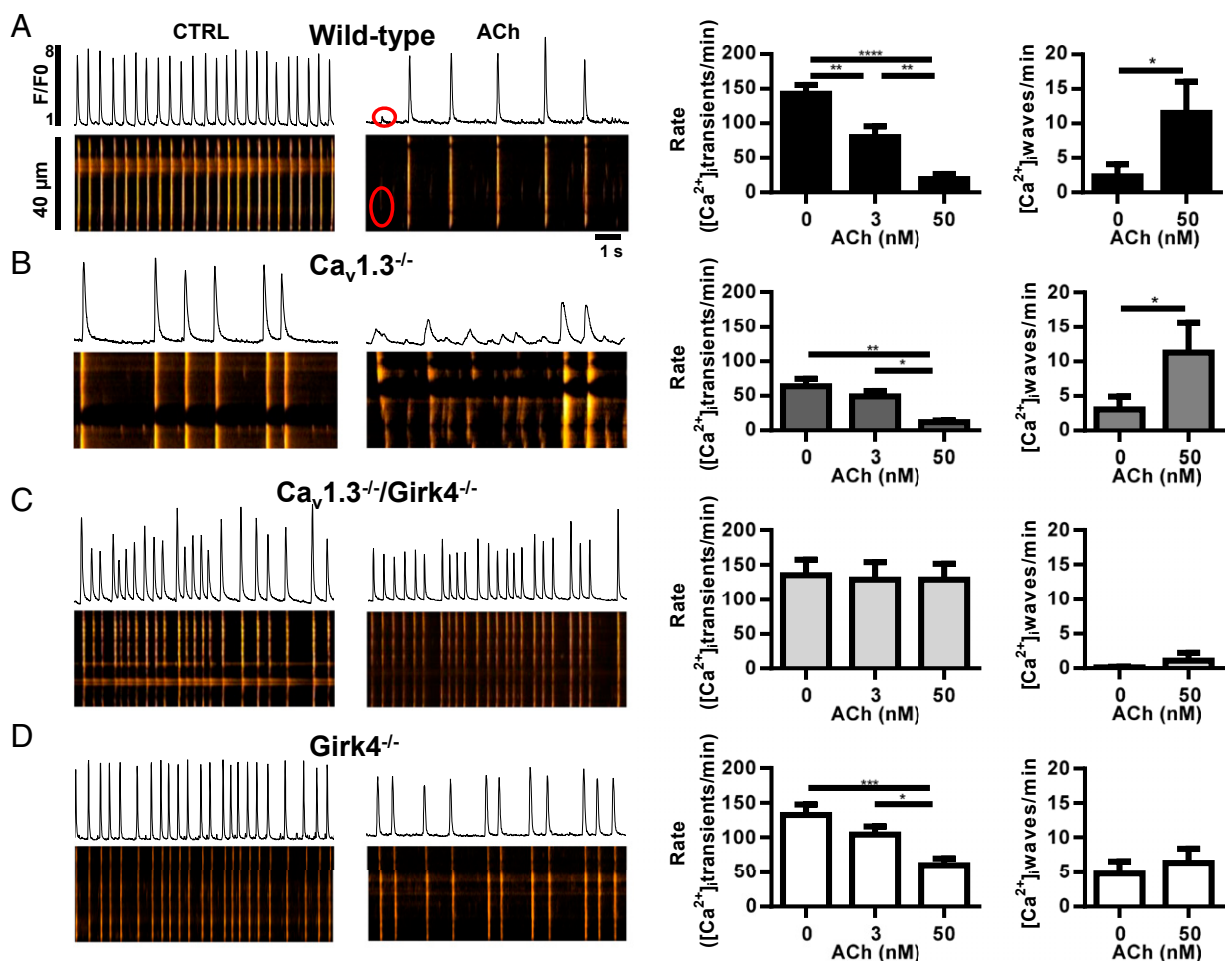
Fig. 7. Suppression of $[Ca^{2+}]_i$ waves in $Ca_v1.3^{-/-}$ SAN myocytes after ablation of I_{KACh}. Sample line scan images (*Left*), averaged frequency of spontaneous $[Ca^{2+}]_i$ transients (*Middle*), and averaged frequency of $[Ca^{2+}]_i$ waves (*Right*) of $n = 11$ WT (*A*), $n = 9$ $Ca_v1.3^{-/-}$ (*B*), $n = 6$ $Ca_v1.3^{-/-}/Girk4^{-/-}$ (*C*), and $n = 12$ $Girk4^{-/-}$ (*D*) SAN myocytes. Statistics: one-way ANOVA followed by Tukey's multiple comparisons test. *$P < 0.05$; **$P < 0.01$; ***$P < 0.001$; ****$P < 0.0001$.

other currents contributing to the diastolic depolarization, such as I_{NCX} (37), $I_{Ca,T}$ (47), and I_f (36), are sufficient to drive normal pacemaker activity (Fig. 8E). This model is consistent also with our evidence showing that I_{KACh} ablation can rescue the slowing of pacemaker activity induced by moderate inhibition of RyR-dependent $[Ca^{2+}]_i$ release of WT, but not $Ca_v1.3^{-/-}$, SAN myocytes (*SI Appendix*, Figs. S9–S11). Indeed, although $Ca_v1.3$-mediated $I_{Ca,L}$ could maintain the balance following concurrent loss of inward I_{NCX} and outward I_{KACh}, additional loss of $Ca_v1.3$-mediated $I_{Ca,L}$ would induce imbalance, and consequently dysfunction of pacemaker activity.

Our evidence indicates that the maintenance of a net inward current in the diastolic phase by I_{KACh} ablation could allow DADs to trigger a full SAN impulse or promote successful AV conduction, thereby preventing SAN pauses and AV block in vivo. $[Ca^{2+}]_i$ waves and DADs thus appear to be a major common arrhythmogenic mechanism in the SAN and cardiac conduction system in both $Ca_v1.3^{-/-}$ mice (this study) and mice carrying silenced cardiac I_f channels (24). This observation is important, because although these two mouse strains both constitute models of bradycardia, their phenotypes are effectively rescued by I_{KACh} ablation, despite presenting different associations with tachycardia-bradycardia syndrome ($Ca_v1.3^{-/-}$) or ventricular arrhythmia (24).

In conclusion, the ability of I_{KACh} ablation to rescue SAN dysfunction and AV block, as well as tachycardia-bradycardia

syndrome and ventricular tachycardia, highlights the clinical potential of I_{KACh} targeting for management of SSS and associated arrhythmias in humans. This study may thus foster pre-clinical research to test I_{KACh} inhibitors in various models of bradycardia and heart block. Importantly, pharmacological inhibitors of I_{KACh} already exist (41, 43). Although these inhibitors have been developed to prevent paroxystic atrial fibrillation, our study suggests that the therapeutic indication of these molecules could be extended to SSS and heart block. Among those compounds, recently described I_{KACh} inhibitors related to the ML297 activator (48) may constitute a potential future pharmacotherapeutical approach for the treatment of SSS.

Materials and Methods

The study conforms to the *Guide for the Care and Use of Laboratory Animals* (49) and to European directives (2010/63/EU), and it was approved by the French Ministry of Agriculture (D34-172-13). An expanded version of the methods is provided in *SI Appendix, Expanded Methods*.

ECG Recording in Conscious Mice. Telemetric recordings of ECGs were performed utilizing a Dataquest A.R.T. recording platform (TA10EA-F20; Data Sciences International) using implantable transmitters as described previously (16). Recordings on sedated mice were performed using a six-lead surface ECG recording device with 25-gauge s.c. electrodes (IOX; EMKA Technologies). Mean heart rate values were obtained in each mouse for an overall 24-h period. For evaluating drug effects, heart rate was recorded for a total period of 8 h. Heart rate before drug injection was averaged over a 2-h period following a 2-h stabilization period. Following drug injection, mean heart
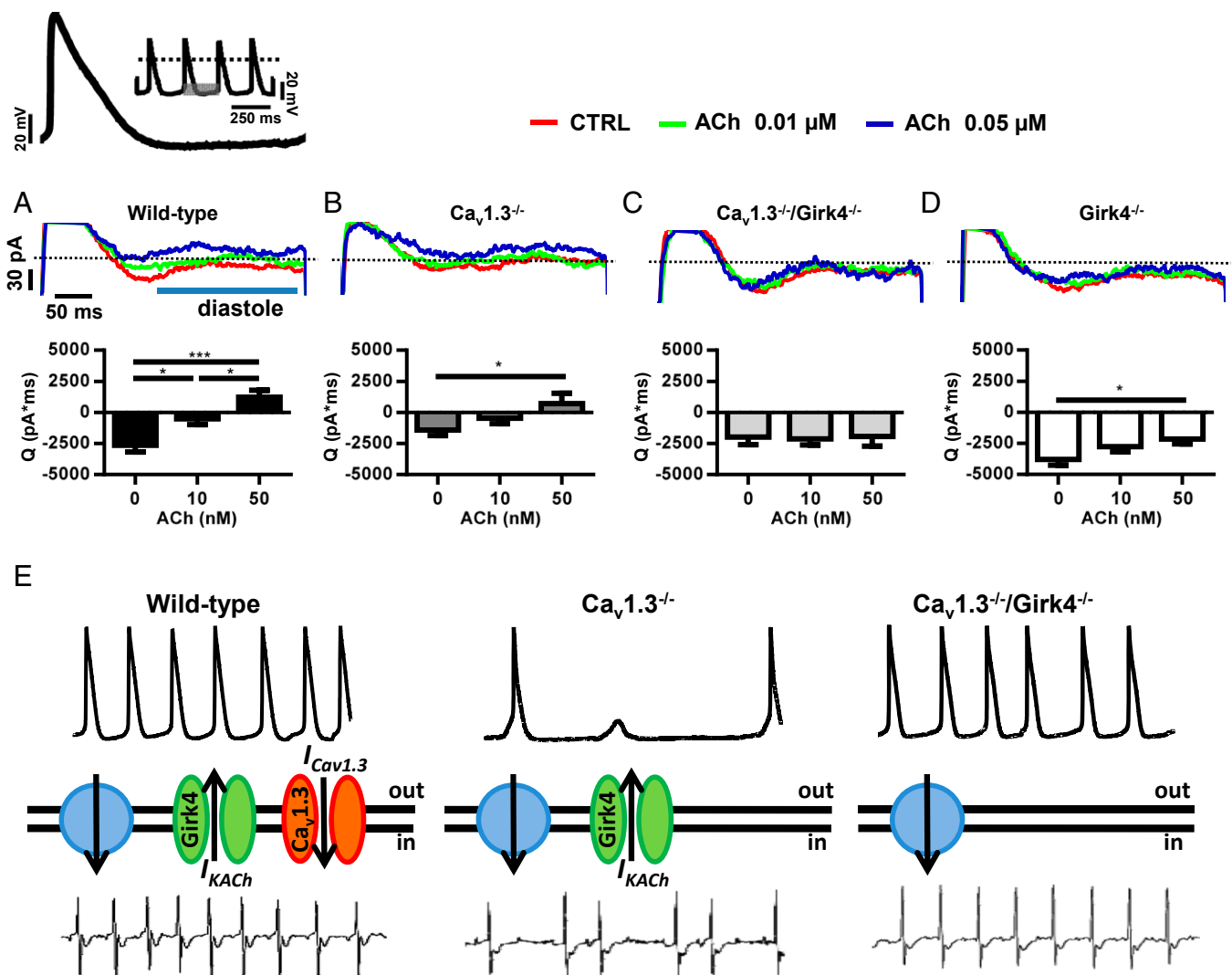
Fig. 8. Diastolic current in isolated $Ca_v1.3^{-/-}$ and $Ca_v1.3^{-/-}/Girk4^{-/-}$ SAN myocytes and heart rate determination. Sample traces (*Upper*) and averaged current time integrals (*Bottom*) measured between the voltage corresponding to the maximum diastolic potential (−61 mV) and the following action potential threshold (−42 mV) of a sample mouse SAN action potential used as voltage-clamp command. Slopes of the linear and exponential parts of the diastolic depolarization were 0.03 and 0.98 mV·ms^{-1}, respectively. (*A, Upper*) Voltage-clamp protocol is shown. Current was measured under control conditions and after perfusion of 0.01 or 0.05 μM ACh in $n = 9$ WT (*A*), $n = 7$ $Ca_v1.3^{-/-}$ (*B*), $n = 16$ $Ca_v1.3^{-/-}/Girk4^{-/-}$ (*C*), and $n = 8$ $Girk4^{-/-}$ (*D*) SAN myocytes. *$P < 0.05$; ***$P < 0.001$. (*E*) Statistics: one-way ANOVA followed by Holm–Sidak's multiple comparisons test. The model of the mechanism of rescue is based on the relationship between the inward-outward current balance that determines the diastolic depolarization and the rate and stability of heart beat. In each panel, sample SAN action potentials (*Top*), functional ionic currents contributing to the diastolic depolarization (*Middle*), and sample ECG recordings (*Bottom*) are shown. The green channel represents I_{KACh}, the red channel represents $Ca_v1.3$-mediated $I_{Ca,L}$ ($I_{Cav1.3}$), and the blue circle shows the idealized sum of other inward currents involved in the pacemaker mechanism (I_{NCX}, I_f, $I_{Ca,T}$). (*Left* to *Right*) Samples of ECG recordings and of pacemaker activity in WT, $Ca_v1.3^{-/-}$, and $Ca_v1.3^{-/-}/Girk4^{-/-}$ mice are shown.

rate values were calculated in each mouse by analyzing periods of 5 min at different time points corresponding to the peak effect of the drug. Heart rates lower than 400 bpm (20% lower than the mean heart rate recorded in WT mice) were defined as "bradycardia." Heart rates lower than 300 bpm (40% lower than the mean heart rate recorded in WT mice) were defined as "deep bradycardia."

Intracardiac Recordings and Pacing in Sedated Mice. For intracardiac explorations, we used a mouse electrophysiology octapolar catheter positioned in the right atrium and ventricle via the right internal jugular vein (Biosense Webster). Surface ECGs were used as a guide for catheter positioning. Pacing was performed with a modified Biotronik UHS20 stimulator and a digital stimulator (DS8000; World Precision Instruments). Standard pacing protocols were used to determine atrial refractoriness and AV conduction parameters and to trigger atrial arrhythmias (*SI Appendix, Expanded Methods*). Atrial tachycardia was defined as a salvo of at least four atrial ectopic beats leading to P waves and atrial electrograms with a shape different from the shapes recorded under sinus rate. We considered atrial tachycardia as non-

sustained when it lasted for less than 10 complexes. We defined atrial fibrillation as an atrial tachyarrhythmia with marked disorganization both on the surface ECG (with no distinguishable P waves) and on the intracardiac recording, with random AV conduction. SAN function was evaluated by measuring the resting SAN cycle length and the SAN recovery time. Atrial pacing was applied for a period of 30 s at cycle lengths of 100 ms and 80 ms. For each pacing cycle length, SAN recovery time was determined as the longest pause from the last paced atrial depolarization to the first SAN return cycle. The SAN conduction time (SACT) was determined with the Narula method, consisting of eight-stimulus trains at a cycle length slightly shorter than the spontaneous SAN cycle length to avoid overdrive suppression. The SACT was also determined by subtracting the intrinsic SAN cycle length from the interval between the last stimulus and the first spontaneous atrial complex.

Recordings on Isolated Langendorff-Perfused Hearts and Isolated SAN Myocytes. Excised hearts were mounted on a Langendorff apparatus (EMKA Technologies). The ECG was continuously recorded by Ag-AgCl electrodes positioned on the epicardial side of the right atrium close to the SAN area and near the apex.

SAN myocytes were isolated as described previously (14). Recordings of action potentials of SAN myocytes were performed using standard patch-clamp techniques.

Imaging of [Ca^{2+}]$_i$. Spontaneous [Ca^{2+}]$_i$ transients were recorded in SAN pacemaker myocytes loaded with Fluo-4 AM (ThermoFisher Scientific) (20 mM, 35 min) at 36 °C. Images were obtained with confocal microscopy (Zeiss LSM 780) by scanning the myocyte with an argon laser in line scan configuration (3.78-ms and/or 1.53-ms line rate); fluorescence was excited at 488 nm, and emissions were collected at >505 nm. A 63× oil immersion objective was used to record [Ca^{2+}]$_i$ in isolated SAN myocytes. Image analyses were performed by ImageJ software (NIH). Images were corrected for the background fluorescence; waves were defined as a [Ca^{2+}]$_i$ release larger than 4 μm and/or with an intrinsic light intensity of >10% of the intensity measured during the following spontaneous [Ca^{2+}]$_i$ transient. Image acquisition and analysis were performed on workstations of the MRI (Plate-forme Régionale d'Imagerie du Languedoc - Roussillon) facility.

Statistical Methods. Results are presented throughout as mean ± SEM. The Student's *t* test, the Fisher's exact test, two-way ANOVA tests followed by Sidak's post hoc tests, or one-way ANOVA tests followed by Tukey's (or Dunnett's) post hoc tests were used to analyze categorical variables. For calculating the level of significance, results were considered significant if $P < 0.05$. In all figures, a single asterisk indicates $P < 0.05$, two asterisks indicate $P < 0.01$, three asterisks indicate $P < 0.001$, and four asterisks indicate $P < 0.0001$. Data were analyzed using GraphPad Prism 6.01 (GraphPad Software).

1. Sanders P, Lau DH, Kalman JK (2014) Sinus node abnormalities. *Cardiac Electrophysiology: From Cell to Bedside*, eds Zipes DP, Jalife J (Elsevier Saunders, Philadelphia), 6th Ed, pp 691–696.
2. Fish FA, Benson DW (2001) Disorders of cardiac rhythm and conduction. *Moss and Adam's Heart Disease in Infants, Children and Adolescents*, eds Allen HD, Clark HP, Gutgesell HP, Driscoll DJ (Lippincott, Williams & Wilkins, Philadelphia), pp 482–533.
3. Semelka M, Gera J, Usman S (2013) Sick sinus syndrome: A review. *Am Fam Physician* 87(10):691–696.
4. Monfredi O, Boyett MR (2015) Sick sinus syndrome and atrial fibrillation in older persons - A view from the sinoatrial nodal myocyte. *J Mol Cell Cardiol* 83:88–100.
5. Mond HG, Proclemer A (2011) The 11th world survey of cardiac pacing and implantable cardioverter-defibrillators: Calendar year 2009–a World Society of Arrhythmia's project. *Pacing Clin Electrophysiol* 34(8):1013–1027.
6. Damani S (2011) When the heart forgets to beat. *Sci Transl Med* 3(76):76ec42.
7. Jensen PN, et al. (2014) Incidence of and risk factors for sick sinus syndrome in the general population. *J Am Coll Cardiol* 64(6):531–538.
8. Rosen MR, Robinson RB, Brink PR, Cohen IS (2011) The road to biological pacing. *Nat Rev Cardiol* 8(11):656–666.
9. Dobrzynski H, Boyett MR, Anderson RH (2007) New insights into pacemaker activity: Promoting understanding of sick sinus syndrome. *Circulation* 115(14):1921–1932.
10. Baig SM, et al. (2011) Loss of Ca$_{(v)}$1.3 (CACNA1D) function in a human channelopathy with bradycardia and congenital deafness. *Nat Neurosci* 14(1):77–84.
11. Le Scouarnec S, et al. (2008) Dysfunction in ankyrin-B-dependent ion channel and transporter targeting causes human sinus node disease. *Proc Natl Acad Sci USA* 105(40):15617–15622.
12. Qu Y, Baroudi G, Yue Y, Boutjdir M (2005) Novel molecular mechanism involving alpha1D (Ca$_v$1.3) L-type calcium channel in autoimmune-associated sinus bradycardia. *Circulation* 111(23):3034–3041.
13. Rose RA, et al. (2011) Iron overload decreases Ca$_V$1.3-dependent L-type Ca^{2+} currents leading to bradycardia, altered electrical conduction, and atrial fibrillation. *Circ Arrhythm Electrophysiol* 4(5):733–742.
14. Mangoni ME, et al. (2003) Functional role of L-type Ca$_v$1.3 Ca^{2+} channels in cardiac pacemaker activity. *Proc Natl Acad Sci USA* 100(9):5543–5548.
15. Chandler NJ, et al. (2009) Molecular architecture of the human sinus node: Insights into the function of the cardiac pacemaker. *Circulation* 119(12):1562–1575.
16. Marger L, et al. (2011) Functional roles of Ca$_v$1.3, Ca$_v$3.1 and HCN channels in automaticity of mouse atrioventricular cells: Insights into the atrioventricular pacemaker mechanism. *Channels (Austin)* 5(3):251–261.
17. Platzer J, et al. (2000) Congenital deafness and sinoatrial node dysfunction in mice lacking class D L-type Ca^{2+} channels. *Cell* 102(1):89–97.
18. Zhang Z, et al. (2005) Functional roles of Ca$_v$1.3(alpha1D) calcium channels in atria: Insights gained from gene-targeted null mutant mice. *Circulation* 112(13):1936–1944.
19. Zhang Z, et al. (2002) Functional Roles of Ca$_v$1.3 (alpha(1D)) calcium channel in sinoatrial nodes: Insight gained using gene-targeted null mutant mice. *Circ Res* 90(9):981–987.
20. Wickman K, Nemec J, Gendler SJ, Clapham DE (1998) Abnormal heart rate regulation in GIRK4 knockout mice. *Neuron* 20(1):103–114.
21. Mesirca P, et al. (2013) The G-protein-gated K$^+$ channel, I$_{KACh}$, is required for regulation of pacemaker activity and recovery of resting heart rate after sympathetic stimulation. *J Gen Physiol* 142(2):113–126.
22. Krapivinsky G, et al. (1995) The G-protein-gated atrial K$^+$ channel I$_{KACh}$ is a heteromultimer of two inwardly rectifying K($^+$)-channel proteins. *Nature* 374(6518):135–141.
23. Bettahi I, Marker CL, Roman MI, Wickman K (2002) Contribution of the Kir3.1 subunit to the muscarinic-gated atrial potassium current I$_{KACh}$. *J Biol Chem* 277(50):48282–48288.
24. Mesirca P, et al. (2014) Cardiac arrhythmia induced by genetic silencing of 'funny' (f) channels is rescued by GIRK4 inactivation. *Nat Commun* 5:4664.
25. Drici MD, Diochot S, Terrenoire C, Romey G, Lazdunski M (2000) The bee venom peptide tertiapin underlines the role of I$_{KACh}$ in acetylcholine-induced atrioventricular blocks. *Br J Pharmacol* 131(3):569–577.
26. Sinnegger-Brauns MJ, et al. (2004) Isoform-specific regulation of mood behavior and pancreatic beta cell and cardiovascular function by L-type Ca^{2+} channels. *J Clin Invest* 113(10):1430–1439.
27. Christel CJ, et al. (2012) Distinct localization and modulation of Ca$_v$1.2 and Ca$_v$1.3 L-type Ca^{2+} channels in mouse sinoatrial node. *J Physiol* 590(Pt 24):6327–6342.
28. Belardinelli L, Giles WR, West A (1988) Ionic mechanisms of adenosine actions in pacemaker cells from rabbit heart. *J Physiol* 405:615–633.
29. Kirchhof P, et al. (2003) Altered sinus nodal and atrioventricular nodal function in freely moving mice overexpressing the A1 adenosine receptor. *Am J Physiol Heart Circ Physiol* 285(1):H145–H153.
30. Lou Q, et al. (2014) Upregulation of adenosine A1 receptors facilitates sinoatrial node dysfunction in chronic canine heart failure by exacerbating nodal conduction abnormalities revealed by novel dual-sided intramural optical mapping. *Circulation* 130(4):315–324.
31. Wakimoto H, et al. (2001) Induction of atrial tachycardia and fibrillation in the mouse heart. *Cardiovasc Res* 50(3):463–473.
32. Kovoor P, et al. (2001) Evaluation of the role of I$_{KACh}$ in atrial fibrillation using a mouse knockout model. *J Am Coll Cardiol* 37(8):2136–2143.
33. Cunha SR, et al. (2011) Defects in ankyrin-based membrane protein targeting pathways underlie atrial fibrillation. *Circulation* 124(11):1212–1222.
34. Lin RJ (2011) Ankyring the heart rhythm. *Sci Transl Med* 3(100):100ec149.
35. Mangoni ME, Nargeot J (2008) Genesis and regulation of the heart automaticity. *Physiol Rev* 88(3):919–982.
36. DiFrancesco D (2010) The role of the funny current in pacemaker activity. *Circ Res* 106(3):434–446.
37. Lakatta EG, Maltsev VA, Vinogradova TM (2010) A coupled SYSTEM of intracellular Ca^{2+} clocks and surface membrane voltage clocks controls the timekeeping mechanism of the heart's pacemaker. *Circ Res* 106(4):659–673.
38. Yue L, et al. (1997) Ionic remodeling underlying action potential changes in a canine model of atrial fibrillation. *Circ Res* 81(4):512–525.
39. Qi XY, et al. (2008) Cellular signaling underlying atrial tachycardia remodeling of L-type calcium current. *Circ Res* 103(8):845–854.
40. Nattel S, Burstein B, Dobrev D (2008) Atrial remodeling and atrial fibrillation: Mechanisms and implications. *Circ Arrhythm Electrophysiol* 1(1):62–73.
41. Hashimoto N, Yamashita T, Tsuruzoe N (2006) Tertiapin, a selective I$_{KACh}$ blocker, terminates atrial fibrillation with selective atrial effective refractory period prolongation. *Pharmacol Res* 54(2):136–141.
42. Wirth KJ, et al. (2007) In vitro and in vivo effects of the atrial selective antiarrhythmic compound AVE1231. *J Cardiovasc Pharmacol* 49(4):197–206.
43. Hashimoto N, Yamashita T, Tsuruzoe N (2008) Characterization of in vivo and in vitro electrophysiological and antiarrhythmic effects of a novel I$_{KACh}$ blocker, NIP-151: A comparison with an I$_{Kr}$-blocker dofetilide. *J Cardiovasc Pharmacol* 51(2):162–169.
44. Cho KI, et al. (2014) Attenuation of acetylcholine activated potassium current I$_{KACh}$ by simvastatin, not pravastatin in mouse atrial cardiomyocyte: Possible atrial fibrillation preventing effects of statin. *PLoS One* 9(10):e106570.
45. Dobrev D, et al. (2005) The G protein-gated potassium current I$_{KACh}$ is constitutively active in patients with chronic atrial fibrillation. *Circulation* 112(24):3697–3706.
46. Voigt N, et al. (2013) Impaired Na$^+$-dependent regulation of acetylcholine-activated inward-rectifier K$^+$ current modulates action potential rate dependence in patients with chronic atrial fibrillation. *J Mol Cell Cardiol* 61:142–152.
47. Mangoni ME, et al. (2006) Bradycardia and slowing of the atrioventricular conduction in mice lacking Ca$_v$3.1/alpha1G T-type calcium channels. *Circ Res* 98(11):1422–1430.
48. Wydeven N, et al. (2014) Mechanisms underlying the activation of G-protein-gated inwardly rectifying K$^+$ (GIRK) channels by the novel anxiolytic drug, ML297. *Proc Natl Acad Sci USA* 111(29):10755–10760.
49. Committee on Care and Use of Laboratory Animals (1996) *Guide for the Care and Use of Laboratory Animals* (Natl Inst Health, Bethesda), DHHS Publ No. (NIH) 85-23.